

Accepted Manuscript

Phosphine oxide and Amino *N*-oxide functionalized phenylquinoline-based small molecules: New cathode interfacial layers for high-performance inverted organic solar cells

Nallan Chakravarthi, Ho-Yeol Park, Um Kanta Aryal, Junyoung Kim, Yeong-Soon Gal, Myungkwan Song, Young-Rae Cho, Sung-Ho Jin

PII: S1566-1199(18)30167-8

DOI: [10.1016/j.orgel.2018.04.011](https://doi.org/10.1016/j.orgel.2018.04.011)

Reference: ORGELE 4619

To appear in: *Organic Electronics*

Received Date: 29 January 2018

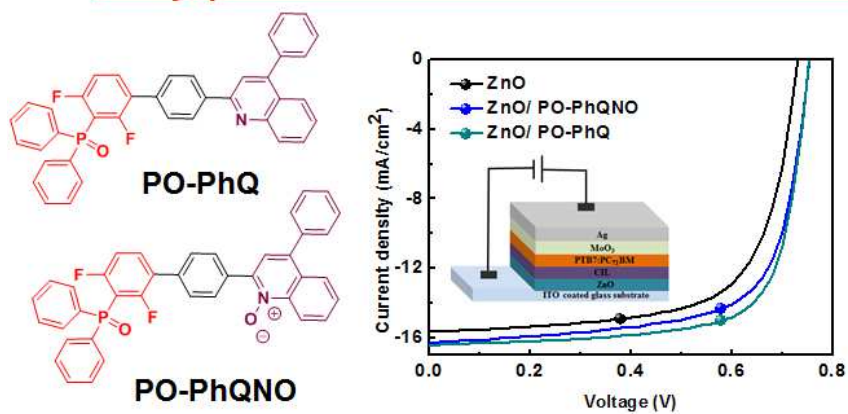
Revised Date: 4 April 2018

Accepted Date: 4 April 2018

Please cite this article as: N. Chakravarthi, H.-Y. Park, U.K. Aryal, J. Kim, Y.-S. Gal, M. Song, Y.-R. Cho, S.-H. Jin, Phosphine oxide and Amino *N*-oxide functionalized phenylquinoline-based small molecules: New cathode interfacial layers for high-performance inverted organic solar cells, *Organic Electronics* (2018), doi: 10.1016/j.orgel.2018.04.011.

This is a PDF file of an unedited manuscript that has been accepted for publication. As a service to our customers we are providing this early version of the manuscript. The manuscript will undergo copyediting, typesetting, and review of the resulting proof before it is published in its final form. Please note that during the production process errors may be discovered which could affect the content, and all legal disclaimers that apply to the journal pertain.



Graphical Abstract**Phenylquinoline based cathode interfacial materials**

Phosphine oxide and Amino N-oxide functionalized Phenylquinoline-based small molecules: New cathode interfacial layers for high-performance inverted organic solar cells

Nallan Chakravarthi ^{a,1}, Ho-Yeol Park ^{a,1}, Um Kanta Aryal ^a, Junyoung Kim ^a, Yeong-Soon Gal ^b, Myungkwan Song ^c, Young-Rae Cho ^{d,*}, Sung-Ho Jin ^{a,*}

^a *Department of Chemistry Education, Graduate Department of Chemical Materials, Institute for Plastic Information and Energy Materials, Pusan National University, Busandaehak-ro 63-2, Busan 46241, Republic of Korea*

^b *Polymer Chemistry Laboratory, College of Engineering, Kyungil University, Gyeongsan, 712-701, Republic of Korea*

^c *Advanced Functional Thin Films Department, Surface Technology Division, Korea Institute of Materials Science (KIMS), 797 Changwondaero, Sungsan-Gu, Changwon, Gyeongnam 642-831, Republic of Korea*

^d *Division of Materials Science and Engineering, Pusan National University, Busandaehak-ro 63-2, Busan 46241, Republic of Korea*

* Corresponding authors.

E-mail addresses: yescho@pusan.ac.kr (Y.-R. Cho), shjin@pusan.ac.kr (S.-H. Jin).

N. Chakravarthi, H.-Y. Park, U. K. Aryal made equal contribution for this article.

ABSTRACT

Two novel small-molecules PO-PhQ and PO-PhQNO, in which both polar phosphine oxide (PO) and *N*-oxide (NO) groups are incorporated in phenyl quinolone core unit were synthesized as efficient cathode interfacial layers (CILs) for inverted organic solar cells (IOSCs). Because of the phenylquinoline (PhQ) group, both PO-PhQ and PO-PhQNO are endorsed with high electron mobility. Due to the presence of polar P=O and N-oxide groups in their molecular structure, PO-PhQ and PO-PhQNO possess good solubility in polar solvents which make them as suitable candidates for interfacial modification of solution processed multilayer IOSCs. As a result, the power conversion efficiency (PCE) of the inverted devices based polythieno[3,4-*b*]-thiophene-co-benzodithiophene (PTB7):(6,6)-phenyl-C₇₁-butyric acid methyl ester (PC₇₁BM) active layer with PO-PhQ and PO-PhQNO as CILs achieve PCE values of 9.03 and 8.53%, respectively, with 10-16 % improvement than that of the control device with ZnO. In addition, both PO-PhQ and PO-PhQNO make certain the IOSC devices with long-term stability. To the best of our knowledge, this is the first time that cathode interfacial materials based on the combination of PhQ and P=O groups is reported. The effective application of these alcohol solution processed CILs indicate that the lending P=O to PhQ could be very promising strategy in developing high performance and eco-friendly solar cells. Our findings would contribute to enhancing the OSC device performances from synthetically view point of designing new materials.

Keywords: Cathode interfacial layers, Phenylquinoline, Phosphine oxide and *N*-oxide, Long-term stability

1. Introduction

The recent advances in molecular engineering have revealed a series of organic solar cell (OSC) potential advantages that may ultimately outbalance the benefits of silicon based solar cells [1-3]. Flexible OSCs have received huge consideration owing to their potential applications as renewable and eco-friendly energy sources and high chances of their large area installation [4,5]. Remarkable progress has been realized for OSCs in achieving power conversion efficiency (PCE), due to the significant accomplishments made in the development of semiconducting π -conjugated materials containing donor-acceptor type polymers and small molecules, and anode/cathode interface engineering [6-8]. Among various key components present in the bulk heterojunction (BHJ) device structure, interfacial layers (ILs) situated between the photoactive layer and charge collecting electrodes, considerably improve the PCE of the corresponding OSCs [9-13]. These ILs act as versatile materials that behaves as electrode surface modifiers/charge injection layers, in such a way that the ILs can control charge recombination at the photoactive layer/electrode interface by blocking the charges to travel in undesired paths [14,15]. But, the lack of key comprehension of the cathode/anode interface modification and surface features restrict their requirement and development [16,17]. Therefore, expanding the class of new, yet efficient ILs and examining the interfacial property are very important for improving OSC device performance.

Various types of ILs made of neutral organic small molecules, alcohol/water-soluble conjugated/non-conjugated polymer electrolytes (CPEs), have been utilized to increase the PCEs of the OSC devices [18-21]. It has been well proven that the phosphine oxide (P=O) and N-oxide end groups in the molecular framework generates encouraging interface dipoles, sequentially reducing the energy barrier for the charge transport via altering the work function of the cathode

[13,22,23]. Additionally, conjugated/non-conjugated polymers with ionic end groups also reduce the work function of the cathode due to the formation of interfacial dipole. However, when compared to that of the polymeric interfacial materials, organic small molecules possess various benefits including synthetic ease, high purity and no problem in batch-to-batch differences.

Generally, phenylquinoline (PhQ) derivatives are used as active electron transporting components for organic light emitting diode applications [24]. These PhQ derivatives, especially poly-(phenylquinoline) are highly thermally robust, photochemically very stable, and shown to have excellent electron accepting properties with high electron affinity, which made them very interesting for OLED applications as an efficient electron transporting materials [25]. On the other hand, P=O based compounds are known to be effective electron transport materials for OLEDs, due to the high electronegativity of the oxygen atom that makes the P=O group highly polar and also show electron withdrawing character [26]. Thus, combining P=O group to PhQ and PhQN-oxide (PhQNO) moieties is an interesting approach to realize new and conceivably better cathode interfacial layers (CILs) with better electron transporting nature. Despite the great achievement in the OSC research field, the cathode interfacial materials explored until now for photovoltaic applications is restricted to a few families. In this scenario, it is of no surprise to mention that the organic small molecules based on the combination of P=O/N-oxide and PhQ groups exemplify a completely unexplored class of materials that could potentially be employed as effective CILs. This class of PhQ-based small molecules offers simple and therefore low-cost synthesis, good solubility in various polar solvents.

Having the idea to expand the family of new CILs, we synthesized two new π -conjugated small-molecules, (2,4-difluoro-4'-(4-phenylquinolin-2-yl)-[1,1'-biphenyl]-3-yl)diphenylphosphine oxide (PO-PhQ) and 2-(3'-(diphenylphosphoryl)-2',4'-difluoro-[1,1'-

biphenyl]-4-yl)-4-phenylquinoline 1-oxide (PO-PhQNO), based on phenyl quinoline moiety and used as CILs for inverted organic solar cells (IOSCs). The molecular structures of PO-PhQ and PO-PhQNO contains P=O and P=O/N-oxide groups respectively in their molecular framework, as shown in Scheme 1. Under standard illumination conditions, optimized IOSCs exhibit a maximum PCE value of 9.03% (PO-PhQ) and 8.53% (PO-PhQNO), which is quite higher than that of the control devices without CILs. The stability test in case of PTB7:PC₇₁BM IOSCs reveal that the existence of PO and PhQ based CILs leads to considerably improved operating lifetimes.

2. Experimental Section

2.1. Materials and measurements

All reagents were purchased from Sigma-Aldrich (Korea) and Solarmer (China) and used without further purification. Moisture-sensitive reactions were conducted in a N₂ atmosphere. The other materials were common chemicals and were used as received. ¹H NMR spectra were recorded on a Varian Mercury Plus 300 MHz spectrometer (USA) in CDCl₃ using tetramethylsilane as an internal reference. The chemical shifts were recorded in ppm related to the singlet of CDCl₃ at 7.26 for ¹H NMR spectroscopy. The UV-visible absorption spectra were recorded on a JASCO V-570 spectrophotometer (USA). Thermal gravimetric analysis was carried out on a Mettler Toledo TGA/SDTA 851e (Switzerland) under N₂ atmosphere at a heating rate of 10 °C min⁻¹ and differential scanning calorimetry (DSC) 822e analyzer under N₂ at a heating rate of 10 °C min⁻¹.

2.2. Device characterization of IOSCs and PSCs

The performances of IOSCs, and PSCs were measured using a calibrated air mass (AM) 1.5 G solar simulator (Oriel Sol3A Class AAA solar simulator, models 94043A (Newport

Stratford, Inc.,USA)) with a light intensity of 100 mW/cm^2 adjusted using a standard PV reference cell ($2 \text{ cm} \times 2 \text{ cm}$ monocrystalline silicon solar cell, calibrated at NREL, Golden, CO) and a computer-controlled Keithley 2400 (Keithley Instruments, Inc. USA) source measure unit. The external quantum efficiency (EQE) spectrum was measured using an Oriel IQE-200 (Newport Stratford, Inc., USA) equipped with a 250-W quartz tungsten halogen lamp as the light source and a monochromator, an optical chopper, a lock-in amplifier, and a calibrated silicon photodetector. While measuring the J - V curves for the OSC devices, a black mask was used and only the effective area of the cell was exposed to light irradiation. Atomic force microscopy (AFM) was used to measure film thickness, roughness, and surface morphologies in tapping mode acquired with a XE-100 (Park System Corp, Korea). All photoemission measurements were carried out in a PHI-5000 Versa Probe II (ULVAC-PHI, Inc. Japan) ultrahigh vacuum surface analysis system equipped with a He-discharge lamp (21.22 eV) and a monochromatic Al $K\alpha$ X-ray. All spectra were measured at a pressure of 1×10^{-6} Pa. Water contact angles were measured using a contact angle 101 measuring system (Plasma systems and materials, Korea).

2.2.1. Fabrication of IOSCs

Indium tin oxide (ITO)-coated glass substrates were cleaned by the process of sonication in acetone, deionized water and IPA sequentially and then dried with N_2 flow. Clean dried samples were treated UV-plasma for 20 minutes. ZnO layer (using ZnO sol-gel precursor) was spin coated with 2,000 rpm for 40 sec (obtained thickness $\sim 45 \text{ nm}$) on the ITO substrate and annealed at $160 \text{ }^\circ\text{C}$ for 15 min. CILs PO-PhQ and PO-PhQNO were spin coated over ZnO layer. CILs were dissolved in 2-methoxy ethanol (2-MOE) with varying concentrations. PTB7:PC₇₁BM (8:12 mg in 1 mL CB with 3% DIO additive) as photoactive layer, was spin coated with rpm 1000 for 40 s and kept for slow dry in covered glass petri dishes at room temperature for 20-30

min. The photoactive layer thickness measured about 100 nm. Finally, MoO₃ (6 nm) layer and Ag (100 nm) layer were thermally evaporated through a shadow mask providing a device active area of 0.11 cm².

2.3. 2-(4-Bromophenyl)-4-phenylquinoline (1)

A mixture of 4-bromoacetophenone (3 g, 15 mmol), 2-aminobenzophenone (3 g, 18 mmol), diphenyl phosphate (3.8 g, 18 mmol), and m-cresol (40 mL) was flushed with N₂ while stirring at room temperature for 30 min and then refluxed for 12 h at 140 °C. The reaction mixture was distilled to remove m-cresol, residue was diluted with MC and washed with 10% sodium hydroxide solution. The reaction mixture was washed with sodium chloride solution and the resulting organic layer was dried over anhydrous MgSO₄ and evaporated the solvent. The residue was then purified by column chromatography on silica gel (hexane:ethyl acetate (EA), 9:1 v/v) to furnish an off-white powder 1 (3.9 g, 54%). ¹H NMR (300 MHz, CDCl₃, δ): 8.21 (d, J = 8.4 Hz, 1H), 8.06 (d, J = 8.4 Hz, 2H), 7.88 (d, J = 8.4 Hz, 1H), 7.75 (s, 1H), 7.71 (dd, J = 7.6, 7.6 Hz, 1H), 7.62 (d, J = 8.4 Hz, 2H), 7.52-7.49 (m, 5H), 7.46 (dd, J = 7.6, 7.6 Hz, 1H). ¹³C NMR (300 MHz, CDCl₃, δ): 155.7, 149.6, 148.9, 138.6, 138.4, 132.1, 130.3, 129.9, 129.7, 129.3, 128.8, 128.7, 126.7, 126.0, 125.9, 124.1, 119.0.

2.4. 2-(2',4'-Difluoro-[1,1'-biphenyl]-4-yl)-4-phenylquinoline (2)

Toluene (20 mL), ethanol (10 mL), and 2M aqueous Na₂CO₃ (12 mL) were added to a mixture of 2-(4-bromophenyl)-4-phenylquinoline (1.5 g, 4 mmol), 2,4-difluorophenylboronic acid (0.65 g, 5 mmol), and tetrakis(triphenylphosphine)palladium (0.125 g, 0.2 mmol). The mixture was refluxed for 12 h under a N₂ atmosphere. After cooling to room temperature, the mixture was extracted with dichloromethane and dried over anhydrous Na₂SO₄. The solvent was removed under reduced pressure and the residue was purified by column chromatography on silica gel

using dichloromethane (MC)/hexane (4:1) as the eluent to produce a white solid. Yield: 55%. ^1H NMR (300 MHz, CDCl_3 , δ): 8.36 (m, 3H), 8.02 (d, 1H), 7.95 (s, 1H), 7.83 (m, 1H), 7.74 (d, 2H), 7.64 (m, 7H), 7.07 (m, 2H). ^{13}C NMR (300 MHz, CDCl_3 , δ): 105.14, 105.48, 105.81, 111.60, 111.65, 111.88, 111.94, 119.66, 119.72, 119.77, 121.33, 121.38, 121.48, 126.03, 129.10, 129.46, 133.69, 133.72, 133.86, 151.51, 151.66, 161.22, 161.39, 163.85, 164.01, 164.74, 164.90, 167.24, 173.49.

2.5. (2,4-Difluoro-4'-(4-phenylquinolin-2-yl)-[1,1'-biphenyl]-3-yl)diphenylphosphine oxide (PO-PhQ)

In a 50-mL three-neck flask, 2-(2',4'-difluoro-[1,1'-biphenyl]-4-yl)-4-phenylquinoline (1 g, 2.5 mmol) was dissolved in 30 mL of THF and the temperature of the reaction was cooled down to $-78\text{ }^\circ\text{C}$. To the reaction mixture, lithium diisopropylamide (2 M, 1.6 mL) was added dropwise, and the temperature of the reaction was maintained at $-78\text{ }^\circ\text{C}$ for another 1 h. Then, 0.54 mL of chlorodiphenylphosphine (0.67 g, 2.8 mmol) was added to the mixture and the solution was stirred overnight. The reaction was quenched with water, extracted with EA, and dried over anhydrous Na_2SO_4 . After removing the solvent, the residue was diluted with 30 mL of MC and 25 mL of hydrogen peroxide solution (30%, w/w), and then stirred at room temperature for 3 h. The crude product was extracted with chloroform (CF) and purified by column chromatography on silica gel using pure EA as an eluent to afford PO-PhQ as white solid. The overall yield was 58%. ^1H NMR (300 MHz, CDCl_3 , δ): 8.24 (m, 1H), 7.94 (d, 1H), 7.85-7.74 (m, 7H), 7.60-7.47 (m, 14H), 7.04 (m, 1H). ^{13}C NMR (300 MHz, CDCl_3 , δ): 112.77, 113.09, 119.19, 125.70, 125.83, 125.99, 126.20, 126.54, 127.73, 128.53, 128.65, 128.70, 129.48, 129.51, 129.57, 129.68, 130.11, 131.13, 131.27, 132.18, 132.21, 133.68, 134.99, 136.08, 138.24, 139.33, 148.78, 149.32, 156.00, 158.83, 164.64, 171.25.

2.6. *2-(3'-(Diphenylphosphoryl)-2',4'-difluoro-[1,1'-biphenyl]-4-yl)-4-phenylquinoline-N-oxide (PO-PhQNO)*

PO-PhQ (1 g, 1.6 mmol) was dissolved in CF (25 mL) and 0.45 g of m-CPBA was slowly added, and stirring was continued overnight at room temperature. Then the reaction mixture was basified with an aqueous KOH solution. The organic layer was separated and dried over anhydrous Na₂SO₄. The solvent was removed under pressure and purified by column chromatography on silica gel using EA/hexane (4:1) as the eluent to produce a yellow solid. Yield: 61%. ¹H NMR (300 MHz, CDCl₃): 8.96 (1H, d), 8.08-8.05 (2H, m), 7.97-7.94 (1H, d), 7.84-7.82 (5H, m), 7.75-7.48 (16H, m), 7.06 (1H, m). ¹³C NMR (300 MHz, CDCl₃, δ): 120.58, 123.43, 126.63, 128.01, 128.53, 128.65, 128.70, 128.82, 128.94, 129.63, 129.89, 130.57, 131.10, 131.24, 132.21, 132.18, 133.20, 133.65, 135.21, 136.07, 137.05, 138.13, 142.27, 143.76.

3. Results and discussion

3.1. Synthesis and characterization

The synthetic routes for the intermediates, PO-PhQ and PO-PhQNO are shown in Scheme S1, and the complete procedures for the synthesis of the CILs are described in the Supporting Information. Initially, 4-bromoacetophenone was treated with 2-aminobenzophenone in the presence of m-cresol to get intermediate 1. Upon treating 2,4-difluorobenzeneboronic acid with compound 1, the difluorophenyl substituted intermediate 2 was obtained. Then the compound 2 was reacted with lithium diisopropylamide and chlorodiphenylphosphine to generate an intermediate which was further used without purification. Upon further oxidation of the unpurified intermediate using hydrogen peroxide, PO-PhQ was attained. Further, PO-PhQ was treated with m-CPBA at room temperature to get PO-PhQNO. Owing to the polar P=O and N-oxide groups, both PO-PhQ and PO-PhQNO are soluble in high polar organic solvents such as

methanol, isopropanol and 2-methoxymethanol. On the other hand, PO-PhQ and PO-PhQNO are also soluble in common organic solvents such as tetrahydrofuran (THF), chloroform (CF), and chlorobenzene (CB). Further, all the intermediates and final products were purified by simple column chromatography, and the chemical structures of the products were characterized by spectroscopic methods. The $^1\text{H-NMR}$ spectra of PO-PhQ and PO-PhQNO complies with the chemical structure, as shown in Fig S1 and S2. The FT-IR spectra of PO-PhQ and PO-PhQNO, shown in Fig. S3a, clearly show a sharp characteristic absorption at 1192 cm^{-1} for the P=O group.

3.2. Thermal, optical and electrochemical properties

The thermal properties of the PO-PhQ and PO-PhQNO were measured by thermal gravimetric analysis (TGA) at a heating rate of $10\text{ }^\circ\text{C}/\text{min}$ (Fig. 1a). The onset of decomposition temperature (T_d , corresponding to 5% weight loss) of PO-PhQ and PO-PhQNO was 320 and $130\text{ }^\circ\text{C}$, respectively. The difference in the decomposition temperatures of PO-PhQ and PO-PhQNO can be well correlated to their molecular structure. The only structural difference in PO-PhQ and PO-PhQNO is that the former compound contains only P=O group and the latter compound contains both P=O and N-oxide groups in the molecular framework. The T_d of PO-PhQNO with single N-oxide group is in agreement with the water soluble naphthalene diimide derivative (NDIO) that possess two terminal N-oxide groups [23]. As shown in Fig. 1b, clear glass transition temperatures (T_g) can be seen from the differential scanning calorimetry (DSC) graphs emerged at approximately 96 and $116\text{ }^\circ\text{C}$ for PO-PhQ and PO-PhQNO, respectively. It is worth stating that the T_g of new CILs is significantly higher than that of well-known electron-transporting material such as bathophenanthroline with T_g value of 66 [13].

The UV–vis absorption spectra of PO-PhQ and PO-PhQNO in diluted CHCl_3 solution and film state are shown in Fig. 1c and d and the absorption maxima values are listed in Table 1. PO-PhQ and PO-PhQNO showed similar absorption profiles both in solution and film states. The absorption maximum of PO-PhQ in film/solution states were found to be at shorter wavelength compared to that of PO-PhQNO, which may be due to relatively less strong withdrawing nature of PO-PhQ. The absorption maxima of PO-PhQ and PO-PhQNO in solution state were observed at 276 and 294 nm, respectively, whereas the absorption maxima of PO-PhQ and PO-PhQNO in film state were found at 286 and 302 nm, respectively. The optical band gap (E_g^{opt}) of PO-PhQ and PO-PhQNO was estimated from the onset absorption edge of the thin film absorption spectra and found to be 3.34 and 2.98, respectively. The highest occupied molecular orbital (HOMO) and energy levels of PO-PhQ and PO-PhQNO were determined using cyclic voltammetry (CV), as shown in Fig. S3b. The HOMO levels of PO-PhQ and PO-PhQNO were observed at -6.08 and -5.73 eV, respectively. The lowest unoccupied molecular orbital (LUMO) levels are calculated from E_g^{opt} and the HOMO energy levels and were found to be -2.74 and -2.75 eV, respectively.

3.3. Photoelectron spectroscopy measurements

Ultraviolet photoelectron spectroscopy (UPS) was used to illustrate the interfacial dipole moment at the ZnO layer surface due to incorporation of PO-PhQ and PO-PhQNO layers. Fig. 2a shows the shift in the secondary cut-off of the ZnO layer after spin-coating the PO-PhQ and PO-PhQNO layers. The schematic diagram of the generation of interfacial dipole due to incorporation of CILs is shown in Fig. 2b. The pristine ZnO film shows a photoemission cutoff at 17.09 eV, which corresponds to a work function (WF) of 4.02 eV. After spin-casting the PO-PhQ and PO-PhQNO layers, the WF value decreases to 3.41 and 3.71 eV respectively. A significant shift in the secondary cut-off of UPS spectra indicates a lowering of the WF of ZnO,

leading to a downward vacuum level shift. This point out that the interfacial dipole moment induced between the ZnO and the photoactive layer increased upon incorporation of PO-PhQ or PO-PhQNO CILs. It is of very important that the Ohmic contact formed at the cathode interface possess much high J_{SC} , therefore the J_{SC} is profoundly linked with the work function change. In the case of PO-PhQ and PO-PhQNO CILs, the improvement in J_{SC} compared to that of the pristine ZnO based devices point out that the effective formation of Ohmic contact at the cathode interface. The WF value of the ZnO layer after insertion of PO-PhQ and PO-PhQNO was 0.61 and 0.31 eV lower than that of the ZnO layer, respectively, indicating that the WF of the ZnO layer after PO-PhQ and PO-PhQNO treatment was shifted by 0.61 and 0.31eV toward the vacuum level. This showed that the interfacial dipole moment formed between the ZnO and the photoactive layer augmented upon the incorporation of PO-PhQ and PO-PhQNO CILs.

3.4. Photovoltaic performance of IOSCs with PO-PhQ and PO-PhQNO CILs

To examine the interfacial modification ability of the new CILs, poly[[4,8-bis[(2-ethylhexyl)oxy]benzo[1,2-b:4,5-b'']dithiophene-2,6-diyl][3-fluoro-2-[(2-ethylhexyl)carbonyl]-thieno[3,4-b]thiophenediyl]] (PTB7):[6,6]-phenyl- C_{71} -butyric acid methyl ester (PC₇₁BM) based IOSCs were fabricated with a device configuration of ITO/ZnO/CIL (PO-PhQ or PO-PhQNO)/PTB7:PC₇₁BM/MoO₃/Ag. The PO-PhQ and PO-PhQNO films were prepared by spin casting the 2-methoxyethanol (2-MOE) on the surface of the photoactive layer. The current density–voltage (J – V) characteristics for IOSCs were measured under AM 1.5G irradiation (100 mW cm⁻²) and are shown in Fig. 3a. The corresponding photovoltaic parameters, including open-circuit voltage (V_{OC}), short-circuit current density (J_{SC}), fill factor (FF), and PCE, estimated from the J – V curves are summarized in Table 2. Various concentrations of CIL were also scrutinized and the optimized one was found to be 0.5 mg/mL for both PO-PhQ and PO-PhQNO.

There are few reports stating that due to the solvent treatment at the interface of the photoactive layer/cathode, there is a chance for the improvement of PCE in IOSCs [27]. In order to avoid any misleading due to the CIL processing solvent (2-MOE), the ZnO layer in the IOSC device was treated with 2-MOE. The control device based on ZnO exhibited a PCE of 7.76%, with V_{OC} of 0.73 V, J_{SC} of 15.67 mA/cm², and FF of 67.66%. When the PTB7:PC₇₁BM film was treated with 2-MOE, the PCE was increased from 7.76% to 7.95%. On the other hand, after incorporating a thin layer of CILs film between the ZnO and photoactive layer, the photovoltaic parameters including FF, J_{SC} , V_{OC} were consecutively improved, in turn giving higher PCE value compared to the pristine ZnO electrode. IOSCs with PO-PhQ and PO-PhQNO revealed the improved PCEs of 8.53% and 9.03%, respectively. It was very clear from Table 1, the PCE increases in the order: ZnO < ZnO/2-MOE < ZnO/PO-PhQNO < ZnO/PO-PhQ. Further to check the reproducibility, ten IOSC devices using the ZnO/PO-PhQ and ZnO/PO-PhQNO bilayer as the CIL were investigated under the same fabrication conditions. The PCE improvement of the devices with PO-PhQ and PO-PhQNO CILs was mostly attributed to the enhanced J_{SC} and FF values (from 15.67 mA/cm², 67.66% (ZnO) to 16.25 mA/cm², 69.57% (ZnO/PO-PhQNO) and 16.41 mA/cm², 72.98% (ZnO/PO-PhQ), indicating that both PO-PhQ and PO-PhQNO CILs reduced the interfacial energy barrier by adjusting the interfacial dipole moment between the ZnO and photoactive layers. As shown in the Fig. S4, the PL quenching was dramatically increased due to the incorporation of PO-PhQ and PO-PhQNO CILs, irrespective of no variation in the absorption spectra of the BHJ blend with ZnO and ZNO/CILs. Hence, it could be confirmed that ZnO/PO-PhQ and ZnO/PO-PhQNO cathode bilayer framework improves the charge transport ability when compared to that of pristine ZnO layer. We fabricated the PSC devices with various concentrations of 0.3-0.8 mg/mL to examine the dependency of PCE on concentration of PO-

PhQ and PO-PhQNO. Interestingly, the PCE of the PO-PhQ and PO-PhQNO based IOSC devices remained at high values of 8.28% and 8.07%, respectively (Table S1 and Fig. S5).

The external quantum efficiency (EQE) spectra of ZnO, ZnO/PO-PhQ, and ZnO/PO-PhQNO based IOSCs are shown in Fig. 3b. All the devices exhibited similar EQE spectra over the wavelength range from 400 to 800 nm. The integrated J_{SC} values estimated from the EQE curves were 15.15, 15.13, 15.36, 16.22 mA/cm² for the pristine ZnO, ZnO/2-MOE, ZnO/PO-PhQ, and ZnO/PO-PhQNO-based IOSC devices, respectively. The integrated J_{SC} values are very well matched with J_{SC} obtained from the J - V measurements. The EQE of the device with the ZnO/PO-PhQ layer showed a noticeable enhancement in the wavelength region ranging from 550 to 700 nm in comparison with the pristine ZnO device, which resulted in higher J_{SC} . As shown in Table 2, the ZnO/CIL-based device has lower series resistance (R_s) than the pristine ZnO or 2-MOE-treated devices. These results clearly confirmed that the PO-PhQ and PO-PhQNO based device possessed the best Ohmic contact at the photoactive layer/cathode interface.

The surface morphologies of the ZnO surface covered with PO-PhQ and PO-PhQNO CILs were investigated using tapping-mode atomic force microscopy (AFM). The root-mean-square (RMS) roughness of the pristine ZnO layer, ZnO/PO-PhQNO and ZnO/PO-PhQ layers were 4.62, 4.32, and 3.98 nm, respectively as shown in Fig. S6. The RMS values point out that the ZnO surface was slightly smoothed due to the presence of PO-PhQ and PO-PhQNO. On the other hand, the surface of the PTB7:PC₇₁BM layer with PO-PhQ and PO-PhQNO layers showed well reduced roughness compared to that of the ZnO on the surface of the photoactive layer. The smoothly modified surfaces of ZnO and PTB7:PC₇₁BM by PO-PhQ and PO-PhQNO, improves the affinity via establishing good contact between the stacked layers (i.e., ZnO

/photoactive layer and photoactive layer/cathode), thus improving the contact. Thus it could be anticipated that the beneficial contacts between the stacked layers enhances the charge transport at the cathode interface (ZnO/photoactive layer) in the IOSC devices to afford a superior PCE for PO-PhQ and PO-PhQNO on the ZnO surface.

We calculated the contact angles and surface energies (γ_s) of the pristine ZnO film and of the ZnO/PO-PhQ and ZnO/PO-PhQNO layers. It is very imperative to know the γ_s values to comprehend the wettability and adhesion properties of an interface. The γ_s values were calculated using the Owens and Wedt geometric mean equation generally used to calculate the surface energy between water and diiodomethane [28,29]. The water contact angles and γ_s values are shown in Table 3. As shown in Fig. 4, the deposition of PO-PhQNO and PO-PhQ layers on the pristine ZnO layer increased the water contact angle from 30.1° to 36.1° and 44.4°, signifying that the ZnO/PO-PhQ and ZnO/PO-PhQNO surfaces became more hydrophobic than the surface of pristine ZnO. The hydrophilic P=O and N-oxide groups of the PO-PhQ and PO-PhQNO layers were seemingly arranged at the ZnO interface, while the hydrophobic conjugated phenyl units containing aromatic framework was present at the photoactive layer surface. The water contact angle results recommended that PO-PhQ and PO-PhQNO layers generated an interfacial dipole moment at the surface of the ZnO layer. Besides the increase in hydrophobicity, the γ_s value of the pristine ZnO layer decreased upon deposition of additional PO-PhQ and PO-PhQNO layers, from 67.3 to 63.1 and 58.2 mN/m, respectively. From the γ_s values, it can be inferred that the electrons that were generated by photoexcitation can be easily moved and ejected from the photoactive layer to the cathode through the PO-PhQ and PO-PhQNO layers. We checked the long-term stability of the IOSC devices for 1000 hours without encapsulation (Fig. S7). The high stability of the PO-PhQ/ZnO and PO-PhQNO/ZnO devices over pristine ZnO may be due to the

superior hydrophobic properties of the CILs, which stopped further entry of water and oxidation into the surface of photoactive layer.

The electron mobility was calculated by using space charge limited current (SCLC) measurements performed in electron-only devices the following diode structure ITO/Al/ZnO/CIL/LiF/Al [30]. The dark J - V curves of the electron-only devices are shown in Fig. S8. The respective electron mobility was calculated according to the Mott-Gurney equation, $J = (9/8) \epsilon_r \epsilon_0 \mu (V^2/L^3)$ where, ϵ_r is the dielectric constant ($\epsilon_r = 3$), ϵ_0 is permittivity of free space. L is the thickness of the ZnO and CILs, μ is the charge mobility, and V is the voltage drop across the device. The ZnO/PO-PhQ and ZnO/PO-PhQNO-based device showed $\mu_{\text{SCLC,e}}$ of $8.15 \times 10^{-5} \text{ cm}^2 \text{ V}^{-1} \text{ s}^{-1}$ and $7.42 \times 10^{-5} \text{ cm}^2 \text{ V}^{-1} \text{ s}^{-1}$, respectively which is two times higher than the $\mu_{\text{SCLC,e}}$ of ZnO with a value of $3.72 \times 10^{-5} \text{ cm}^2 \text{ V}^{-1} \text{ s}^{-1}$. The $\mu_{\text{SCLC,e}}$ results are well lined up with higher FF and the improved dark current (forward bias), as shown in Fig. 4a. The mobility results specify that the incorporation of PO-PhQ and PO-PhQNO layers on ZnO surface developed the interfacial contact between the ZnO and the photoactive layer, thus increasing the PCE in the ZnO/PO-PhQ and ZnO/PO-PhQNO-based devices.

The dark J - V characteristics of PTB7:PC₇₁BM blends with or without CILs on ZnO surface were shown in Fig. 5a. The series resistance (R_s) for the corresponding devices are shown in Table 2. The incorporation of CILs on the ZnO surface reduced R_s for PO-PhQ from 2.01 to 1.48 Ωcm^2 and for PO-PhQNO from 2.01 to 1.76 Ωcm^2 . The R_s results could give a valid reason for the experimental enhancement in J_{SC} , from 15.67 to 16.41 mA/cm^2 for PO-PhQ and from 15.67 to 16.25 mA/cm^2 for PO-PhQNO. The R_{SH} values of pristine ZnO, ZnO/PO-PhQ, and ZnO/PO-PhQNO were 5.46×10^3 , 2.12×10^4 and $1.12 \times 10^4 \Omega\text{cm}^2$, respectively, demonstrating that the ZnO combined with PhQ based CILs had a lower leakage current and excellent diode

characteristics. These features elevated the FF of pristine ZnO from 67.66 to 72.98% and 69.57%, respectively for ZnO/PO-PhQ, and ZnO/PO-PhQNO bilayers. The surface modification by PO-PhQ and PO-PhQNO improves hydrophobicity of ZnO film (Fig. 4a) owing to the aromatic hydrocarbon moieties out of ZnO surface, leading to a better contact to photoactive active layer, which is consistent with electrical impedance spectrum (EIS) results (Fig. 5b). The extracted contact resistance of PO-PhQ or PO-PhQNO modified ZnO (ZnO/PO-PhQ and ZnO/PO-PhQNO) film is found to be remarkably reduced, facilitating electron transport to ITO electrode. This result in conjunction with the abovementioned increased electron mobility will be remarkable significant for the increase of photocurrent in IOSC devices.

4. Conclusion

In summary, we developed two novel PhQ-based alcohol-soluble π -conjugated organic small molecules, PO-PhQ and PO-PhQNO as an efficient CIL to modify the ZnO surface in BHJ IOSCs. The UPS studies revealed that the polar groups (P=O and N-oxide) in the new CIL molecules play a critical role in reducing the energy barrier by generating interfacial dipole at the cathode interface. The contact angle and surface energy results reveal both PO-PhQ and PO-PhQNO reduced the surface energy and increased the hydrophobic nature thus improving both interfacial contacts and wettability between the ZnO and photoactive layer. The CILs enhanced the electron collection efficiency of the IOSC devices and modified the rough ZnO surface to a smoother surface, thus enriched the PCE and stability. Even though the donor-acceptor type polymers were incorporated to enable the impact of PO-PhQ and PO-PhQNO as CILs in BHJ IOSCs, it is anticipated that these CILs could deliver extraordinary PCE in perovskite solar cells in various types of device configurations via solution process. Further, the research outcome

reported in this work could motivate additional interest in this type of organic small molecules based on PhQ for optoelectronic applications.

Acknowledgments

This work was supported by National Research Foundation (NRF-2016R1E1A1A01942593) by the Ministry of Science, ICT & Future Planning, Republic of Korea.

Appendix A. Supplementary material

Supplementary data associated with this article can be found, in the online version, at <http://dx.doi.org/>

References

- [1] G. Li, R. Zhu, Y. Yang, Polymer solar cells, *Nat. Photonics*. 6 (2012) 153.
- [2] T. R. Andersen, H. F. Dam, B. Andreasen, M. Hösel, M. V. Madsen, S. A. Gevorgyan, R. R. Søndergaard, M. Jørgensen, F. C. Krebs, A rational method for developing and testing stable flexible indium- and vacuum-free multilayer tandem polymer solar cells comprising up to twelve roll processed layers, *Sol. Energy Mater. Sol. Cells* 120 (2014) 735.
- [3] B. C. Thompson, J. M. Frechet, Polymer-fullerene composite solar cells, *Angew. Chem. Int. Ed.*, 47 (2008) 58.
- [4] Y.-J. Cheng, S.-H. Yang, C.-S. Hsu, Synthesis of conjugated polymers for organic solar cell applications, *Chem. Rev.*, 109 (2009) 5868.
- [5] P. M. Beaujuge, J. M. Frechet, Molecular design and ordering in π -functional materials for transistor and solar cell applications, *J. Am. Chem. Soc.*, 133 (2011) 20009.
- [6] W.-C. Zhao, D.-P. Qian, S.-Q. Zhang, S.-S. Li, O. Inganäs, F. Gao, J. Hou, Fullerene-free polymer solar cells with over 11% efficiency and excellent thermal stability, *Adv. Mater.*, 28 (2016) 4734.

- [7] Z. He, B. Xiao, F. Liu, H. Wu, Y. Yang, S. Xiao, C. Wang, T. P. Russell, Y. Cao, Single-junction polymer solar cells with high efficiency and photovoltage, *Nat. Photonics.*, 9 (2015) 174.
- [8] Y. Cui, H. Yao, B. Gao, Y. Qin, S. Zhang, B. Yang, C. He, B. Xu, J. Hou, Fine-tuned photoactive and interconnection layers for achieving over 13% efficiency in a fullerene-free tandem organic solar cell, *J. Am. Chem. Soc.*, 139 (2017) 7302.
- [9] J. R. Manders, S.-W. Tsang, M. J. Hartel, T.-H. Lai, S. Chen, C. M. Amb, J. R. Reynolds, F. So, Solution-processed Nickel Oxide hole transport layers in high efficiency polymer photovoltaic cells, *Adv. Funct. Mater.*, 23 (2013) 2993.
- [10] S.-H. Liao, Y.-L. Li, T.-H. Jen, Y.-S. Cheng, S.-A. Chen, Multiple functionalities of polyfluorene grafted with metal ion-intercalated crown ether as an electron transport layer for bulk-heterojunction polymer solar cells: Optical interference, hole blocking, interfacial dipole, and electron conduction, *J. Am. Chem. Soc.*, 134 (2012) 14271.
- [11] J.-H. Seo, A. Gutacker, Y.-M. Sun, H.-B. Wu, F. Huang, Y. Cao, U. Scherf, A. J. Heeger, G. C. Bazan, Improved high-efficiency organic solar cells via incorporation of a conjugated polyelectrolyte interlayer, *J. Am. Chem. Soc.*, 133 (2011) 8416.
- [12] H. Azimi, T. Ameri, H. Zhang, Y. Hou, C. O. R. Quiroz, J. Min, M. Hu, Z.-G. Zhang, T. Przybilla, G. J. Matt, E. Spiecker, Y. Li, C. J. Brabec, A universal interface layer based on an amine-functionalized fullerene derivative with dual functionality for efficient solution processed organic and perovskite solar cells, *Adv. Energy Mater.* 2015, 1401692.
- [13] W.-Y. Tan, R. Wang, M. Li, G. Liu, P. Chen, X.-C. Li, S.-M. Lu, H. L. Zhu, Q.-M. Peng, X.-H. Zhu, W. Chen, W. C. H. Choy, F. Li, J. Peng, Y. Cao, Lending triarylphosphine oxide to phenanthroline: a facile approach to high-performance organic small-molecule cathode

interfacial material for organic photovoltaics utilizing air-stable cathodes, *Adv. Funct. Mater.* 24 (2014) 6540.

[14] H.-L. Yip, A. K. Y. Jen, Recent advances in solution-processed interfacial materials for efficient and stable polymer solar cells, *Energy Environ. Sci.*, 5 (2012) 5994.

[15] T. Kirchartz, T. Agostinelli, M. Campoy-Quiles, W. Gong, J. J. Nelson, Understanding the thickness-dependent performance of organic bulk heterojunction solar cells: The influence of mobility, lifetime, and space charge, *J. Phys. Chem. Lett.*, 3 (2012) 3470.

[16] G. F. A. Dibb, T. Kirchartz, D. Credgington, J. R. Durrant, J. Nelson, Analysis of the relationship between linearity of corrected photocurrent and the order of recombination in organic solar cells, *J. Phys. Chem. Lett.*, 2 (2011) 2407.

[17] I. Lange, J. Kniepert, P. Pingel, I. Dumsch, S. Allard, S. Janietz, U. Scherf, D. Neher, Correlation between the open circuit voltage and the energetics of organic bulk heterojunction solar cells, *J. Phys. Chem. Lett.*, 4 (2013) 3865.

[18] Z. He, C. Zhong, X. Huang, W. Y. Wong, H. Wu, L. Chen, S. Su, Y. Cao, Simultaneous enhancement of open-circuit voltage, short-circuit current density, and fill factor in polymer solar cells, *Adv. Mater.*, 23 (2011) 4636.

[19] Y. Zhou, C. Fuentes-Hernandez, J. Shim, J. Meyer, A. J. Giordano, H. Li, P. Winget, T. Papadopoulos, H. Cheun, J. Kim, M. Fenoll, A. Dindar, W. Haske, E. Najafabadi, T. M. Khan, H. Sojoudi, S. Barlow, S. Graham, J.-L. Bredas, S. R. Marder, A. Kahn, B. Kippelen, A universal method to produce low-work function electrodes for organic electronics. *Science* 336 (2012) 327.

- [20] X. Guan, K. Zhang, F. Huang, G. C. Bazan, Y. Cao, Amino N-oxide functionalized conjugated polymers and their amino-functionalized precursors: New cathode interlayers for high-performance optoelectronic devices, *Adv. Funct. Mater.*, 22 (2012) 2846.
- [21] B. Meng, Y. Fu, Z. Xie, J. Liu, L. Wang, Phosphonate-functionalized donor polymer as an underlying interlayer to improve active layer morphology in polymer solar cells, *Macromolecules* 47 (2014) 6246.
- [22] N. Chakravarthi, K. Gunasekar, W. Cho, D. X. Long, Y.-H. Kim, C. E. Song, J.-C. Lee, A. Facchetti, M. Song, Y.-Y. Noh, S.-H. Jin, A simple structured and efficient triazine-based molecule as an interfacial layer for high performance organic electronics, *Energy Environ. Sci.* 9 (2016) 2595.
- [23] K. Zhao, L. Ye, W. Zhao, S. Zhang, H. Yao, B. Xu, M. Sun, J. Hou, Enhanced efficiency of polymer photovoltaic cells via the incorporation of a water-soluble naphthalene diimide derivative a cathode interlayer, *J. Mater. Chem. C*, 3 (2015) 9565.
- [24] C. J. Tonzola, M. M. Alam, B. A. Bean and S. A. Jenekhe, New soluble n-type conjugated polymers for use as electron transport materials in light-emitting diodes, *Macromolecules* 37 (2004) 3554.
- [25] A. P. Kulkarni, C. J. Tonzola, A. Babel, S. A. Jenekhe, Electron transport materials for organic light-emitting diodes, *Chem. Mater.*, 16 (2004) 4556.
- [26] Z.-G. Wu, J. Zhou, L. Yu, G. Karotsis, Y. Wang, Y.-X. Zheng, Y. Pan, Novel phosphine oxide-based electron-transporting materials for efficient phosphorescent organic light-emitting diodes, *J. Mater. Chem. C*, 5 (2017) 8579.

- [27] N. Chakravarthi, K. Gunasekar, C. S. Kim, D.-H. Kim, M. Song, Y. G. Park, J. Y. Lee, Y. Shin, I.-N. Kang and S.-H. Jin, Synthesis, characterization and photovoltaic properties of 4,8-dithienylbenzo[1,2-*b*:4,5-*b'*]dithiophene-based donor–acceptor polymers with new polymerization and 2D conjugation extension pathways: A potential donor building block for high performance and stable inverted organic solar cells, *Macromolecules* 48 (2015) 2454.
- [28] B. J. Moon, G. Y. Lee, M. J. Im, S. Song, T. Park, In situ modulation of the vertical distribution in a blend of P3HT and PC₆₀BM via the addition of a composition gradient inducer, *Nanoscale* 6 (2014) 2440.
- [29] D. K. Owens, R. C. Wendt, Estimation of the surface free energy of polymers, *J. Appl. Polym. Sci.*, 13 (1969) 1741.
- [30] H. Cha, G. Y. Lee, Y. Fu, Y. J. Kim, C. E. Park, T. Park, Simultaneously grasping and self-organizing photoactive polymers for highly reproducible organic solar cells with improved efficiency, *Adv. Energy Mater.*, 3 (2013) 1018.

Scheme Captions

Scheme 1. Design strategy for the design of phenylquinoline-based new interlayers (PO-PhQ, PO-PhQNO).

Figure Captions

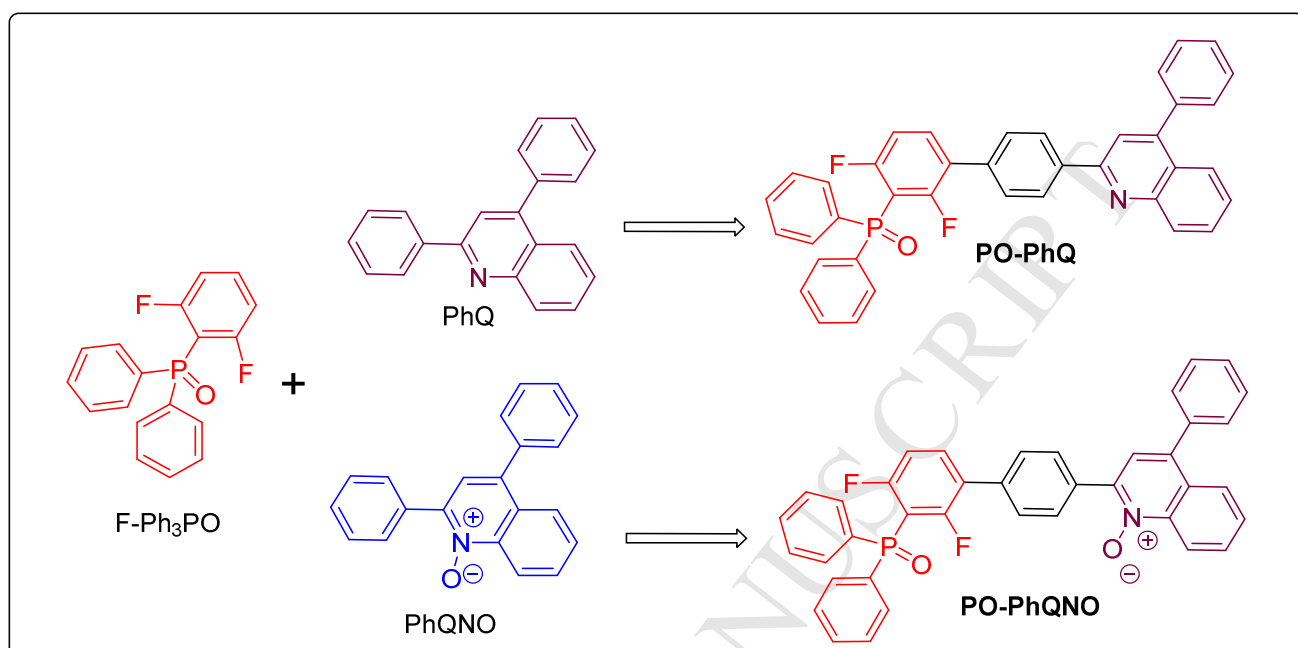
Fig. 1. (a) TGA curves of PO-PhQ and PO-PhQNO, (b) DSC curves of PO-PhQ and PO-PhQNO, (c) UV-vis absorption spectra of PO-PhQ and PO-PhQNO in CF solution, and (d) thin film state.

Fig. 2. (a) UPS spectra of the ZnO layer, before and after deposition of PO-PhQ and PO-PhQNO, (b) The schematic energy diagram of interfacial dipole of the ZnO and the ZnO/CIL thin layers.

Fig. 3. (a) $J-V$ and (b) EQE spectra of PTB7:PC₇₁BM-based IOSCs of the ZnO and PO-PhQ/ZnO, and ZnO/PO-PhQNO thin layers, respectively, under AM 1.5 G irradiation (100 mW cm⁻²).

Fig. 4. Water and diiodomethane contact angles of ZnO, ZnO/PO-PhQ, and ZnO/PO-PhQNO surfaces.

Fig. 5. (a) $J-V$ characteristics of PTB7:PC₇₁BM-based PSCs on top of the ZnO and PO-PhQ/ZnO, and ZnO/PO-PhQNO thin layers in the dark and (b) Nyquist plots of devices with/without CILs under the AM 1.5 illumination.



Scheme 1. Design strategy for the design of phenylquinoline-based new interlayers (PO-PhQ, PO-PhQNO).

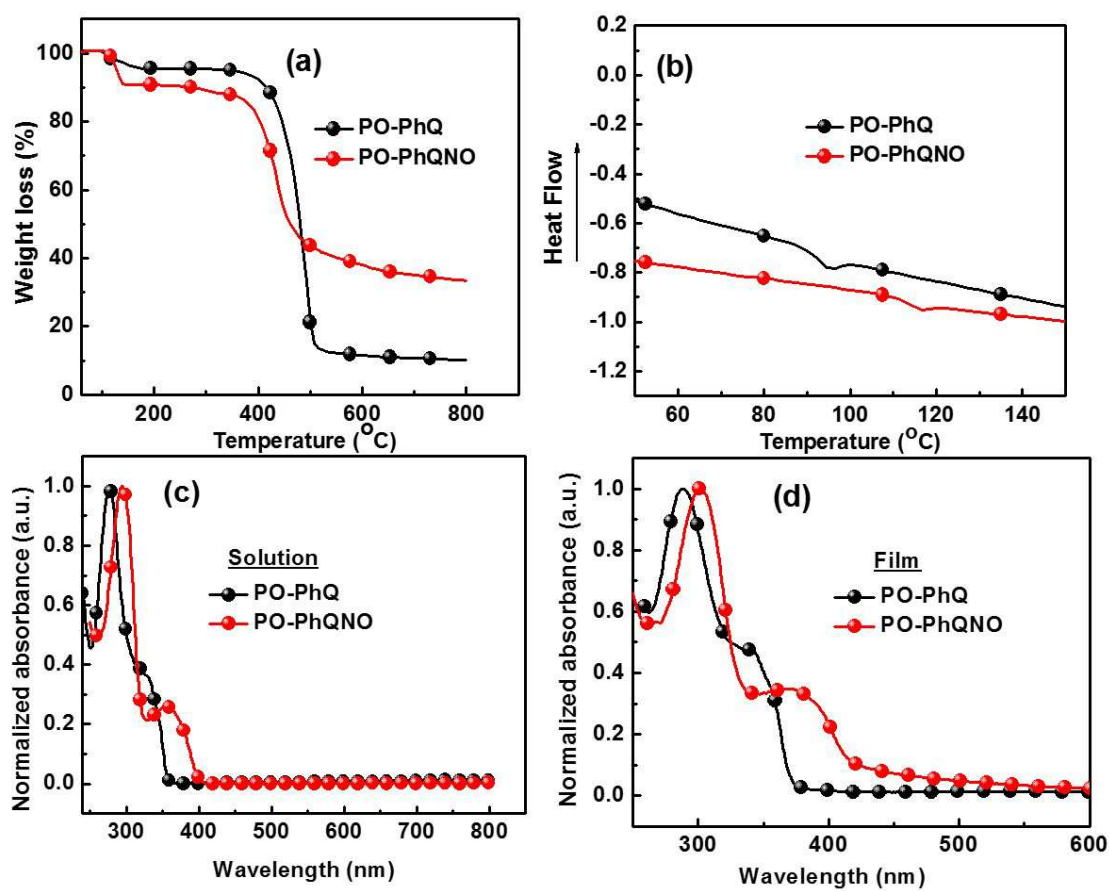


Fig. 1. TGA curves of PO-PhQ and PO-PhQNO, (b) DSC curves of PO-PhQ and PO-PhQNO, (c) UV-vis absorption spectra of PO-PhQ and PO-PhQNO in CF solution, and (d) thin film state.

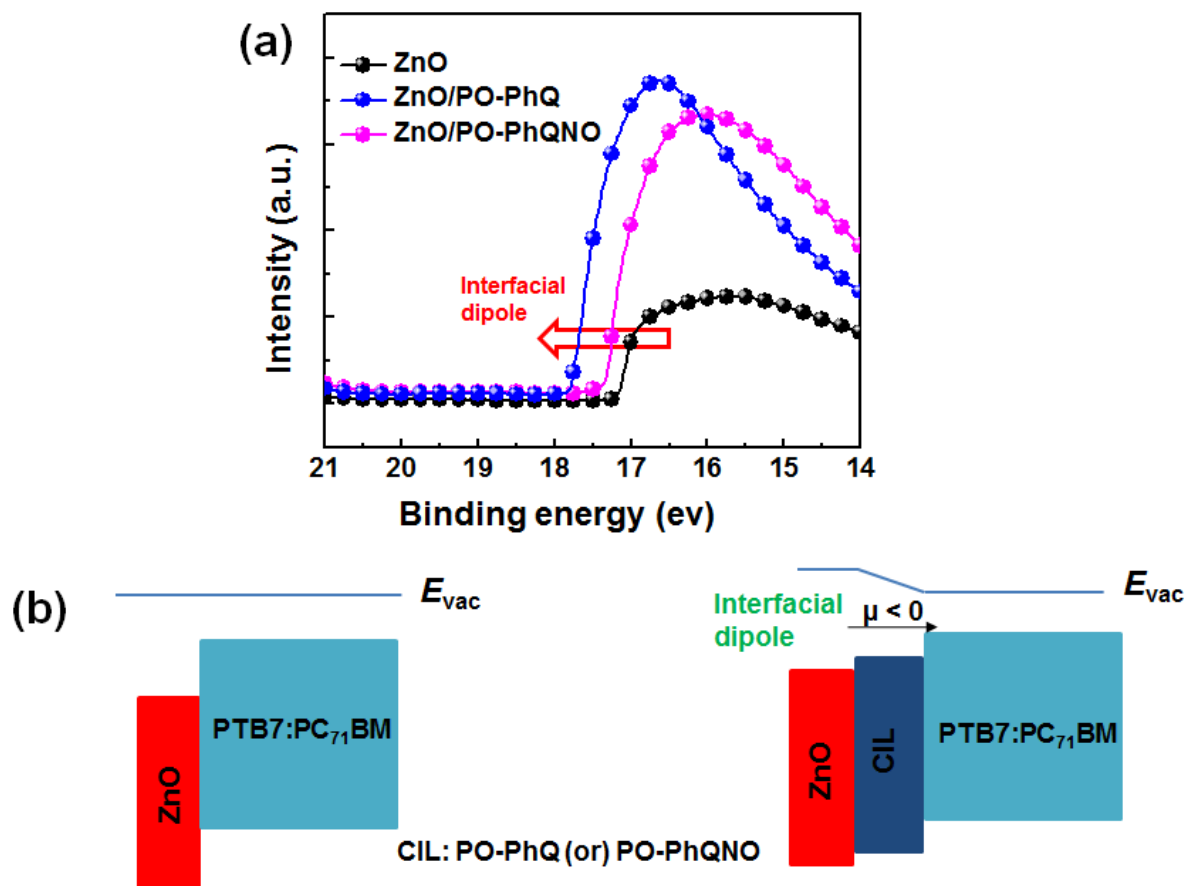


Fig. 2. a) UPS spectra of the ZnO layer, before and after deposition of PO-PhQ and PO-PhQNO, (b) The schematic energy diagram of interfacial dipole of the ZnO and the ZnO/CIL thin layers.

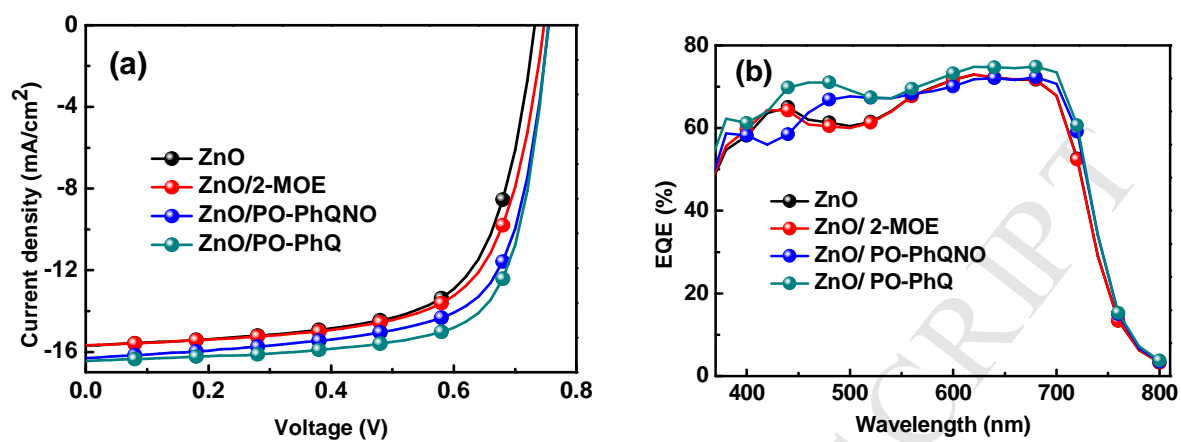


Fig. 3. (a) J - V and (b) EQE spectra of PTB7:PC₇₁BM-based IOSCs of the ZnO and PO-PhQ/ZnO, and ZnO/PO-PhQNO thin layers, respectively, under AM 1.5 G irradiation (100 mW cm⁻²).

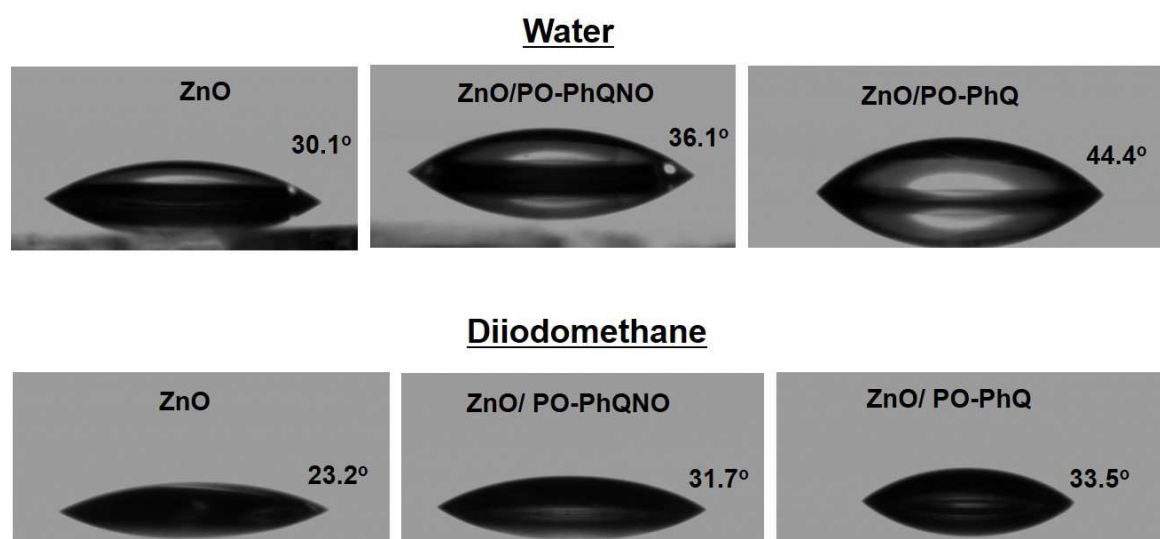


Fig. 4. Water and diiodomethane contact angles of ZnO, ZnO/PO-PhQ, and ZnO/PO-PhQNO surfaces.

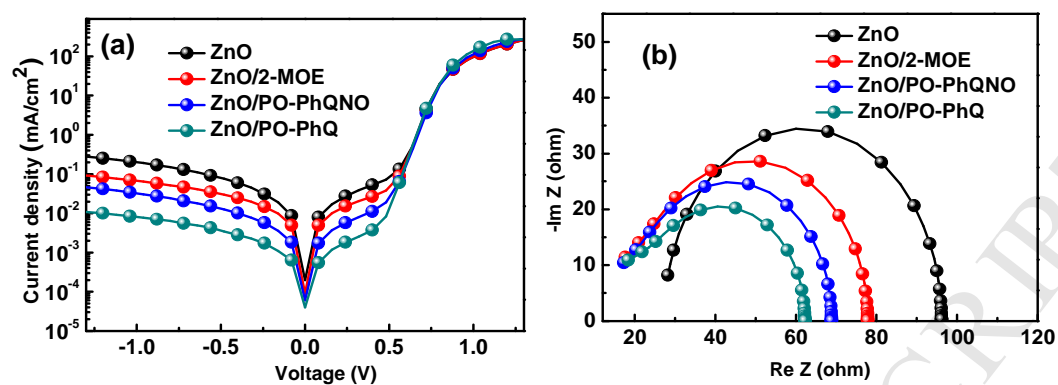


Fig. 5. J - V characteristics of PTB7:PC₇₁BM-based PSCs on top of the ZnO and PO-PhQ/ZnO, and ZnO/PO-PhQNO thin layers in the dark and (b) Nyquist plots of devices with/without CILs under the AM 1.5 illumination.

Table 1

Thermal, optical and electrochemical properties of PO-PhQ and PO-PhQNO.

CIL	T_d	T_g	Solution λ_{\max} (nm) ^a	Film λ_{\max} (nm) ^b	E_g^{opt} (eV) ^c	HOMO (eV)	LUMO (eV)
PO-PhQ	320	96	276	286	3.34	-6.08	-2.74
PO-PhQNO	130	116	294	302	2.98	-5.73	-2.75

^aAbsorption maxima measured from UV-visible absorption spectrum in CF solution.^bAbsorption maxima measured from UV-visible absorption spectrum in thin film state.^cEstimated from the onset of the absorption in thin films ($E_g^{\text{opt}} = 1240/\lambda_{\text{onset}}$).

Table 2

Photovoltaic performance of PTB7:PC₇₁BM-based PSCs with or without CIL under AM 1.5G Irradiation (100 mW cm⁻²).

Device	V_{oc} (V)	J_{sc} (mA/cm ²)	FF (%)	PCE (%)	Integrated J_{sc} (mA/cm ²)	R_s [Ω Cm ²]
ZnO	0.73	15.67	67.66	7.76	15.15	2.01
ZnO/2-MOE	0.74	15.66	68.02	7.95	15.13	1.95
ZnO/PO-PhQNO	0.75	16.25	69.57	8.53	15.36	1.76
ZnO/PO-PhQ	0.75	16.41	72.98	9.03	16.22	1.48

Table 3

Contact angle and surface energy data of ZnO and ZnO/CIL surfaces.

Film	θ (H ₂ O) (Degree)	θ (CH ₂ I ₂) (Degree)	γ^{da} (mJ m ⁻²)	γ^{pb} (mJ m ⁻²)	$\gamma^s = (\gamma^{da} + \gamma^{pb})$ (mJ m ⁻²)
ZnO	30.1	23.2	36.3	31.0	67.3
ZnO/PO-PhQNO	36.1	31.7	33.7	29.4	63.1
ZnO/PO-PhQ	44.4	33.5	33.9	24.3	58.2

γ^s : Surface energy, γ^{da} : Dispersion of surface tension, γ^{pb} : Polar component of surface tension

Highlights

- Two new phenylquinoline based cathode interfacial materials were synthesized.
- Polar P=O and N-oxide pendant groups are present in CIM molecular structure
- Achieved high PCE of 9.03% and 8.53% for PO-PhQ and PO-PhQNO, respectively.
- PO-PhQ and PO-PhQNO based devices showed good long term stability.